Bull Volcanol (1995) 57:85–98

ORIGINAL PAPER

L. G. Mastin

Thermodynamics of gas and steam-blast eruptions

Received: July 4, 1994 / Accepted: November 30, 1994

Abstract Eruptions of gas or steam and non-juvenile debris are common in volcanic and hydrothermal areas. From reports of non-juvenile eruptions or eruptive sequences world-wide, at least three types (or end-members) can be identified: (1) those involving rock and liquid water initially at boiling-point temperatures ('boiling-point eruptions'); (2) those powered by gas (primarily water vapor) at initial temperatures approaching magmatic ('gas eruptions'); and (3) those caused by rapid mixing of hot rock and ground- or surface water ('mixing eruptions'). For these eruption types, the mechanical energy released, final temperatures, liquid water contents and maximum theoretical velocities are compared by assuming that the erupting mixtures of rock and fluid thermally equilibrate, then decompress isentropically from initial, near-surface pressure ($\leqslant$10 MPa) to atmospheric pressure. Maximum mechanical energy release is by far greatest for gas eruptions ($\leqslant \sim 1.3$ MJ/kg of fluid–rock mixture) – about one-half that of an equivalent mass of gunpowder and one-fourth that of TNT. It is somewhat less for mixing eruptions ($\leqslant \sim 0.4$ MJ/kg), and least for boiling-point eruptions ($\leqslant \sim 0.25$ MJ/kg). The final water contents of erupted boiling-point mixtures are usually high, producing wet, sloppy deposits. Final erupted mixtures from gas eruptions are nearly always dry, whereas those from mixing eruptions vary from wet to dry. If all the enthalpy released in the eruptions were converted to kinetic energy, the final velocity (v_{max}) of these mixtures could range up to 670 m/s for boiling-point eruptions and 1820 m/s for gas eruptions (highest for high initial pressure and mass fractions of rock (m_r) near zero). For mixing eruptions, v_{max} ranges up to 1150 m/s. All observed eruption velocities are less than 400 m/s, largely because (1) most solid material is expelled when m_r is high, hence v_{max} is low; (2) observations are made of large blocks the velocities of which may be less than the average for the mixture; (3) heat from solid particles is not efficiently transferred to the fluid during the eruptions; and (4) maximum velocities are reduced by choked flow or friction in the conduit.

Key words Thermodynamics · Gas eruptions · Steam-blast eruptions

Larry G. Mastin
US Geological Survey, Cascades Volcano Observatory,
5400 MacArthur Boulevard, Vancouver, WA 98661, USA.
Tel.: 360 6967518. Fax: 360 696-7866

Introduction

The term 'eruption' generally implies the expulsion of magma and magmatic gases from a vent in the earth. Yet a large percentage of eruptions, perhaps the majority, do not expel juvenile magma but only fragments of non-juvenile rock entrained in a mixture of gas, steam or liquid water. Such eruptions have been given a variety of names, including 'phreatic' eruption, implying that heated groundwater is the driving fluid (e.g. Stearns and MacDonald 1946), 'hydrothermal' eruption or explosion when fluids from a pre-existing hydrothermal system are thought to be involved (Muffler et al. 1971; Nairn and Wiradiradja 1980; Hedenquist and Henley 1985), 'gas' eruption when gas or superheated water vapor is considered to be driving force, or 'steam-blast' eruption when steam from an unspecified source is responsible (Jaggar 1949).

Although non-juvenile eruptions are generally smaller than magmatic or phreatomagmatic eruptions, they are not necessarily less violent. Relative to the amount of ejecta released, the violence displayed by some non-juvenile eruptions is as great as that of some magmatic and phreatomagmatic eruptions. Eruptive velocities of large, non-juvenile gas and steam-blast eruptions (150–200+ m/s) are comparable with those of most large magmatic or phreatomagmatic eruptions. Well-developed base surge deposits, although not recognized at most non-juvenile eruptive centers, can be extensive at some sites (e.g. McPhie et al. 1990; Nairn

1979). The purpose of this paper is to use published accounts of eruptions and the basic principles of thermodynamics to identify controls on the violence of non-juvenile eruptions.

All eruptions, whether juvenile or non-juvenile, are powered by essentially the same process: the conversion of thermal energy contained in the erupting mixture to mechanical energy, in forms such as acceleration and lifting of debris, seismic waves and shock waves as the mixture is ejected. The violence of an eruption therefore depends largely on two factors: (1) the amount of energy available in the erupting fluid/solid mixture and (2) the efficiency of conversion of this energy to mechanical work. The amount of energy available depends in turn on such factors as the initial temperature and pressure of the mixture, the fluid phase (liquid or vapor) or proportions of coexisting phases and the amount of solid debris. For magmas in the shallow subsurface, the temperature, pressure and water content are reasonably well constrained, allowing relatively easy estimates of the thermal energy content. Numerous papers have calculated the total energy, maximum theoretical velocities, plume heights, dynamics of volcanic blasts or jets and other phenomena by assuming the efficient conversion of thermal energy to mechanical energy (e.g. Fisher and Schmincke 1984, Ch. 4).

For non-juvenile eruptions, the range of initial temperatures, pressures and solid contents is much broader than for magmatic eruptions. This, in large part, is responsible for their wide range of eruptive styles. The energetics and dynamics of non-juvenile eruptions are generally less well understood, although for the subset of non-juvenile eruptions involving the ejection of water and rock, initially at boiling-point temperatures, investigators as early as the 1950s (White 1955; Goguel 1956) used the basic principles of thermodynamics to estimate mechanical energy release, final temperatures and mass fractions of steam versus liquid in these mixtures. Numerous workers (e.g. Muffler et al. 1971; Hedenquist and Henley 1985; Moyer and Swanson 1987; Mastin 1991; Marini et al. 1993) have since used the same approach to estimate the energetics of specific steam-blast eruptions. Two studies have attempted to model the dynamics of these eruptions (Dowden et al. 1991; Bercich and McKibbin 1992). At least two other types of non-juvenile eruptions are well-documented in the literature, but their thermodynamics have not been as well studied: those powered by volcanic gas and rock at near-magmatic temperatures; and those that result from the rapid mixing of hot, non-juvenile rock with external water. The former are similar to magmatic eruptions except that the solid fraction is non-magmatic and the relative proportions of rock and gas are more variable. The latter are analogous to phreatomagmatic eruptions except that the thermal energy of the solid material is much more variable. The objective of this paper is to extend the thermodynamic analysis of non-juvenile eruptions to include initial conditions that correspond to those of all three eruption types. A major conclusion of this study is that these three types of eruptions may produce significant differences in energy release, maximum velocity and deposit characteristics.

Types of gas and steam-blast eruptions

Type I, or 'boiling-point' eruptions

Of all non-juvenile eruptions reported world-wide, a significant percentage occur in areas of known hydrothermal activity (e.g. Muffler et al. 1971; Hedenquist and Henley 1985; Nelson and Giles 1985; Bixley and Browne 1988). The areas studied by these workers in particular, as well as most other liquid-dominated hydrothermal areas, contain zones in which water temperatures are at or near the boiling point for their pressure. In such zones, the depressurization of the water will lead to explosive boiling and expansion analogous to boiler explosions in industrial situations. Geyser eruptions are the best known (and most photographed; Fig. 1a) examples of boiling-point eruptions, though they generally expel little, if any, solid material. Larger eruptions have been triggered by a variety of mechanisms, including: (1) rapid draining of lakes overlying shallow thermal aquifers (Muffler et al. 1971); (2) fluid pressure reduction during geothermal production (Bixley and Browne 1988); and (3) sealing of upflow zones (Zlotnicki et al. 1992), in some instances followed by the development of a cap of overpressured, non-condensable gases (Hedenquist and Henley 1985).

Outside developed hydrothermal areas, the initial state of fluids involved in steam-blast eruptions is generally unknown, although boiling-point conditions are arguably the most likely initial thermodynamic state. One reason for this inference is that, due to the large enthalpy of phase change, water temperatures remain at the boiling point throughout a large range of energy input. A second reason is that, once the boiling point is reached, additional heating of water can more readily lead to increases in fluid volume or pressure that may trigger an eruption.

Well-documented boiling-point eruptions have ranged in length from minutes (e.g. Old Faithful) to days (Marinelli 1969). Maximum eruptive velocities range up to at least 150 m/s from direct observations (Le Guern et al. 1980), or to 200+ m/s from ballistic analyses (Nairn and Wiradiradja 1980). Deposit volumes range up to at least 10^7 m^3 at Kawerau, New Zealand (Nairn and Wiradiradja 1980). The deposits of boiling-point eruptions consist mostly of poorly sorted, matrix-supported mixtures of angular to subrounded clasts with bedding absent or indistinct (e.g. White 1955; Muffler et al. 1971; Hedenquist and Henley 1985; Browne and Lloyd 1986). Signs of abundant water, in the form of muddiness of the deposits (White 1955) or post-depositional liquefaction and mobilization (Lloyd and Keam 1974; Marini et al. 1993) are common,

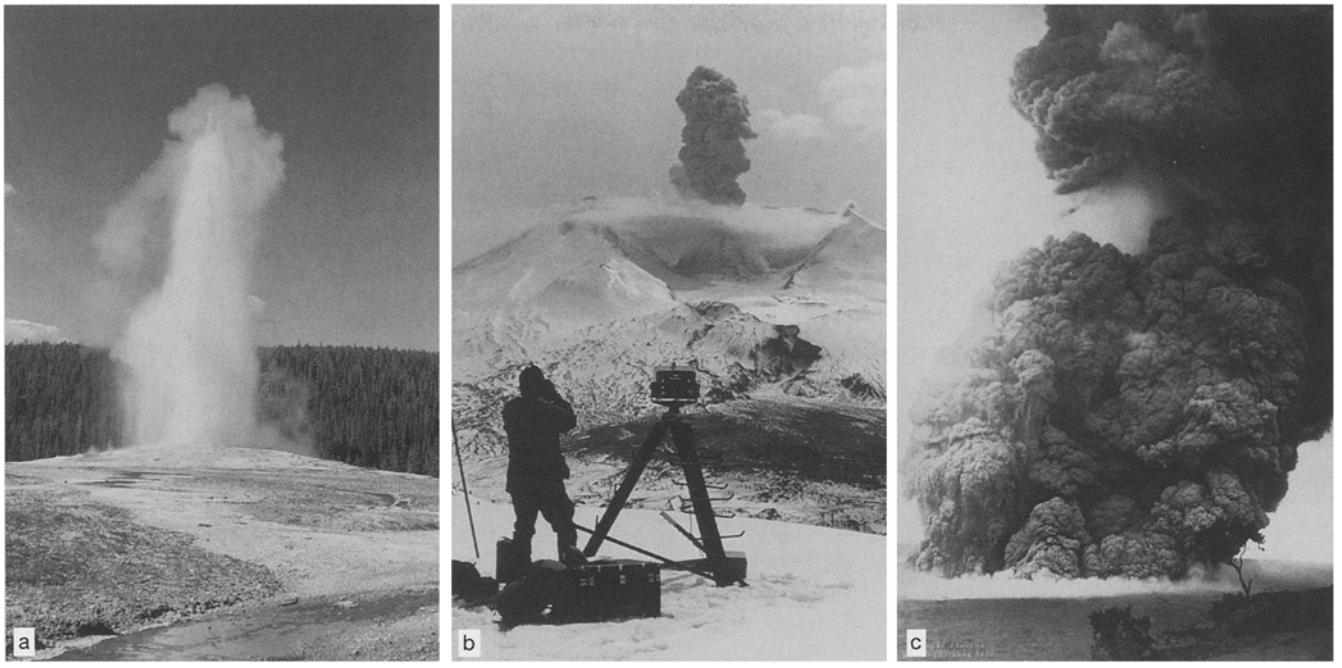

Fig. 1a–c Examples of three types of non-juvenile eruptions described in this paper. **a** Eruptions caused by rapid decompression of compressed water under boiling-point conditions. The best known of these are geysers (shown here is Old Faithful), but eruptions of boiling-point water from much greater depth (e.g. at Kawerau, New Zealand: Nairn and Wiradiradja 1980) have produced up to 10×10^6 m^3 of solid ejecta. **b** Eruption of gas and debris from Mount St Helens Dome in 1983. Such eruptions are driven by the expulsion of magmatic gas (primarily water vapor) and entrained solid debris. **c** Eruption caused when hot, non-juvenile rock mixes with external water. The one shown took place at Halemaumau Crater, Hawaii, in May 1924. Photos by **a** Carolyn Driedger, **b** Lyn Topinka and **c** K. Maehara

though the stages of some eruptions (Lloyd and Keam 1974) have produced relatively dry deposits. The dry deposits are presumably produced during the expulsion of steam which has separated from the liquid water, as occurs in the latter stages of geyser eruptions (White 1967; Ingebritsen and Rojstaczer 1993). With a few possible exceptions (e.g. Nairn and Wiradiradja 1980), steam-blast eruptions from boiling-point geothermal systems do not produce well-developed, cross-bedded base-surge deposits. The most voluminous steam-blast eruption on record from a liquid-dominated hydrothermal system, at Rotomahana, New Zealand in 1886 produced $\sim 5 \times 10^7$ m^3 of deposits with abundant dry base surges, but the high emplacement temperature of its deposit (hot enough to ignite some trees) suggests that fluid temperatures were raised above boiling by magmatic heat (Nairn 1979).

Type II, or 'gas' eruptions

Burnham (1979) pointed out that the energy content of gases exsolved during the crystallization of magmas would be more than sufficient to power non-juvenile eruptions. Magma bodies exsolve voluminous amounts of gas as they ascend, due to the reduction in gas solubility with reduced pressure. A cubic kilometer of water-saturated silicic magma ascending from 5 to 1 km depth, for example, could release enough water vapor (~ 2 wt.%; Burnham 1979) to occupy 3 km^3 at 10 MPa pressure. (Assuming a magma density of 2500 kg/m^3, 2 wt.% of water from 1 km^3 of melt would amount to 5×10^{10} kg water. Given the specific volume of water vapor (0.06 m^3/kg at 950° C, 10 MPa), this amounts to 3×10^9 m^3, or 3 km^3 water vapor). Cooling and crystallization of magma cause additional volatile exsolution, albeit at a slower rate than during ascent.

It is primarily in systems where gas escape is periodically blocked that gas explosions occur. Such non-juvenile gas explosions have been referred to as 'ultravulcanian' by MacDonald (1972). At Galeras Volcano, Colombia (Stix et al. 1993), periodic blockage of gas exsolved from a shallow magma body apparently led to a series of violent eruptions since 1989, including one that killed six volcanologists and nine tourists in January 1993. At Mount St Helens, Mastin (1994) hypothesized that non-juvenile eruptions on the lava dome in 1989–1991 were caused by rainstorms that triggered the episodic release of accumulated gas below the still-hot dome.

Many gas eruptions fall into a gray area between juvenile and non-juvenile eruption types. Included among these are explosions of exsolved gas on lava domes (Fink et al. 1992) that eject relatively young dome rock. Many hundreds of small eruptions on the Mount St Helens lava dome in the early- and mid-1980s (Fig. 1b) may have been of this type. The initial stages of certain vulcanian eruptions (e.g. Self et al. 1979), triggered by the rupture of a cap of cooled magma

above a gas chamber below, may also fall into this category (though the later stages of many such eruptions are undeniably juvenile). Within this gray area, the distinction between juvenile and non-juvenile eruptions becomes unimportant; the primary energy source for these eruptions, regardless of the composition of the solid fraction, is compressed gas.

Gas eruptions are characterized by a relatively high explosivity, short duration and a relatively small amount of debris ejected. The best-documented eruptions (e.g. Galeras, Smithsonian Institution 1992) have begun abruptly, with the highest velocities and greatest output of solid debris (especially large, ballistic blocks) occurring during the throat-clearing stage, and have ended gradually, with jetting of nearly ash-free gas from the vent. At Asama Volcano in Japan, deposits ejected during the initial stages of explosive eruptions in 1935–1941 primarily consisted of ballistic blocks (Minakami 1942), as did explosions at Galeras (Smithsonian Institution 1992) and Mount St Helens (Mastin 1994). Typical eruption durations are on the order of minutes (Smithsonian Institution 1992, 1993), although relatively ash-free gas can be expelled for a few hours afterward (Smithsonian Institution 1993).

Type III, or 'mixing' eruptions

Steam-blast eruptions caused by mixing of hot rock with water are fundamentally the same as phreatomagmatic eruptions except that the rock is non-juvenile and may be at temperatures below magmatic. Two types of mixing eruptions have been described: (1) those caused by mixing of groundwater and hot country rock in a collapsed eruptive conduit and (2) rootless explosions triggered when erupted volcanic debris contacts ground- or surface water.

Mixing eruptions caused by conduit collapse. The best-documented conduit-collapse eruptions took place on Kilauea Volcano, Hawaii, in May 1924 (Decker and Christiansen 1984; Fig. 1c). These blasts expelled debris from a crater (Halemaumau) that had contained an active lava lake for decades until shortly before the explosions began. In spring 1924, the lava lake drained and disappeared from view (200 m below the crater rim) four days before the first eruption. Up to 13 explosions per day, lasting from a few minutes to seven hours, continued for 18 days, ejecting ash clouds up to 2 km in the air and blocks more than 1 m in diameter nearly 1 km from the crater (Decker and Christiansen 1984). The blocks ranged in temperature from ambient to barely incandescent at night ($>700°$ C). Some of the dust from the explosion was hot enough to emit a dull red glow as it cleared the crater rim (Finch 1943).

The circumstances leading up to this eruption suggest that it was caused when groundwater and hot country rock cascaded into the conduit as it was drained of magma. The mixing process was probably stimulated by magma surges, which were detected during the steam explosions by harmonic tremor (Finch 1943). An older and much larger eruption in 1790 (Decker and Christiansen 1984; McPhie et al. 1990) is also hypothesized to have been caused when groundwater and hot country rock invaded an eruptive vent at the volcano's summit. The last stage expelled about 4×10^7 m^3 of entirely non-juvenile debris (McPhie et al. 1990) – more than any other documented non-juvenile eruption except that in 1886 at Rotomahana – and produced well-bedded surge deposits that extend at least 3 km from the eruptive vent.

Other eruptions that may have been caused by conduit-collapse and mixing of water with hot country rock include pre-1790 steam-blasts on Kilauea (Decker and Christiansen 1984) and recent eruptions on Mount Etna, including one in 1979 that killed nine tourists and injured 23 (Kiefer 1981).

Rootless eruptions through pyroclastic flows and lava flows. The term 'secondary hydroeruptions' was coined by Moyer and Swanson (1987) to describe rootless eruptions that vent through pyroclastic-flow deposits when they cover surficial water, then heat and vaporize it. Dozens of secondary hydroeruptions blasted through pyroclastic-flow deposits that ponded in the North Fork Toutle River Valley following the 18 May and 12 June 1980 eruptions of Mount St Helens (Moyer and Swanson 1987). Similar hydroeruptions followed pyroclastic-flow emplacement at Krakatau, 1883 (Francis and Self 1983), Novarupta, 1912 (Hildreth 1983), Crater Lake, Oregon, 6600 BP (Bacon 1983), Mount Pelee, 1929–1932 (Perret 1937) and Mount Pinatubo, 1991 (Wolfe and Hoblitt, in press). Rootless eruptions have also been documented where basalt flows have covered wet ground (Long 1989).

Most hydroeruptions at Mount St Helens followed emplacement of the pyroclastic flows by a few hours to days, though some did not erupt until weeks, months or, in a few cases, more than a year after the deposits were laid down. The eruptions ranged in violence from fumarolic degassing, to fountaining, to explosive cratering (Moyer and Swanson 1987).

Secondary hydroeruptions at Mount Pinatubo have continued sporadically since the June 1991 climactic eruption (Wolfe and Hoblitt in press). They have generated tephra plumes exceeding 18 km altitude that disrupt air traffic to Manila and have been mistaken at times for primary eruptions by the press and local residents. Some eruptions remobilize hot deposits into secondary pyroclastic flows that travel as far as 8 km down-valley. At least two causal mechanisms are cited by Wolfe and Hoblitt for these eruptions: (1) collapse of banks of hot pyroclastic material into streams and (2) invasion of groundwater into hot deposits along buried stream channels. The latter type have produced craters tens to hundreds of meters in diameter (those at Mount St Helens are about 5–100 m in diameter, Moyer and Swanson 1987).

Along with mixing eruptions caused by conduit collapse, secondary hydroeruptions are the only type of non-juvenile eruption that consistently produce well-developed, cross-bedded surge deposits. One boiling-point eruption (Nairn and Wiradiradja 1980) and a few other non-juvenile eruptions whose place in this three-type classification scheme are unknown (Nairn 1979; Nairn et al. 1979) have also produced such deposits. Some secondary eruptions at Mount St Helens produced crescent-shaped surge dunes up to 1 m high around their vents that show evidence for both wet and dry depositional conditions. Less violent eruptions produced massive or plane parallel bedded deposits resulting from fountaining of debris (Moyer and Swanson 1987).

Theory

Gas and steam-blast eruptions exhibit a wide range of eruptive styles. In all cases, however, the erupting mixture starts from a subsurface position at a pressure and temperature greater than ambient atmospheric conditions (Fig. 2). During the eruption, the mixture is transported to the surface over a period of time ranging from a fraction of a second to perhaps on the order of 10 seconds (for eruptive conduits tens to hundreds of meters long and eruptive velocities of tens to hundreds of meters per second). Upon reaching the surface, the mixture expands rapidly to atmospheric pressure. Thermal equilibration, on the other hand, takes place over a much longer period of time. It is therefore convenient

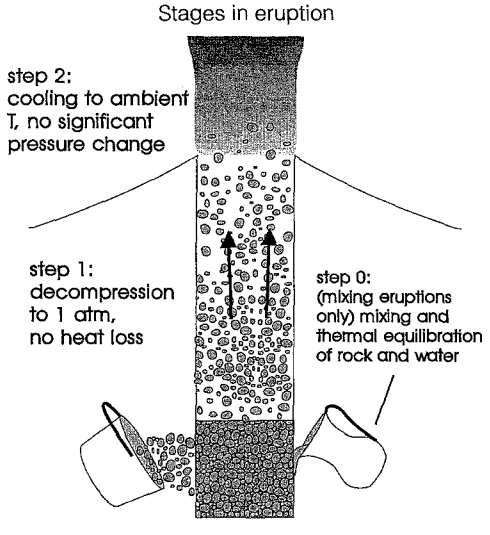

Fig. 2 For purposes of analysis, the energy released in gas and steam-blast eruptions has been divided up into the steps illustrated in this figure. Step 1: hot liquid water and (or) water vapor and rock, initially in thermal equilibrium with one another, at $P_i > 1$ atm and $T_i \geq$ the boiling point of water, rapidly decompress during ejection to the surface, with no significant heat loss. Step 2: following decompression, the fluid and rock cool to ambient conditions at atmospheric pressure. (Step 0: for mixing eruptions, hot rock and water are assumed to mix and equilibrate thermally prior to decompression)

to divide up the energy released by an eruption into two steps: (1) a 'decompression' step, in which the mixture of rock and water is decompressed from subsurface to atmospheric conditions with little or no heat transfer to the surroundings and (2) a 'cooling' step, in which the expelled mixture gradually comes into thermal equilibrium with ambient conditions. The mechanical energy released during the decompression step accounts for all phenomena that we normally associate with an explosion: seismic wave generation, production of shock waves in the atmosphere, acceleration and lifting of debris in the gas thrust portion of the eruptive column and so on. The mechanical energy released during the cooling stage includes primarily convective uplift, turbulence in the eruptive plume, lightning generation and other high-level atmospheric phenomena. In this paper, we are primarily concerned with energy released in the decompression stage.

Thermodynamics of decompression

The mechanical energy released during decompression is equal to the change in internal energy (U) of the erupting mixture

$$\text{Available mechanical energy} = U_{mi} - U_{mf} \quad (1)$$

where U_{mi} and U_{mf} are the initial and final total internal energies of the mixture of rock and fluid expelled during the eruption. Evaluation of the change in energy per kilogram of mixture, or specific internal energy (u), gives an indication of the potential violence of an eruption per mass of erupting material.

At any stage during decompression, the specific internal energy (u_m) of a rock/fluid mixture is simply the sum of the specific internal energies of each component (u_r and u_w for rock and water, respectively), times their respective mass fractions (m_r and m_w)

$$u_m = m_r u_r + m_w u_w \quad (2)$$

The specific internal energy of rock, which is considered chemically inert and incompressible for this study, is simply

$$u_r = \int_{T=0}^{T=T_i} C_r \, dT \quad (3)$$

where T is the absolute temperature (in Kelvin) of the rock, C_r is the specific heat of the rock and T_i is the temperature of the mixture before decompression. By assuming that C_r is roughly constant with temperature [at ~1 kJ/(kg K)], Equation (3) can be simply stated as $u_r = C_r T$.

The specific internal energy of the fluid is given by the following equation

$$u_w = x u_{wv} + (1 - x) u_{wl} \quad (4)$$

where x is the mass fraction of steam in the fluid component and u_{wl} and u_{wv} are the specific internal ener-

gies of the liquid and vapor phases under the given thermodynamic conditions. The specific internal energies of liquid water and steam have been tabulated from extensive experimental data (e.g. Haar et al. 1984). For this study, I assume that the erupted fluid consists of pure H_2O with no other components (CO_2, SO_2, H_2S, etc.). For a given initial thermodynamic state (defined by initial pressure, temperature and proportions of liquid water and steam), the specific internal energy and other state variables, including entropy, are calculated using a Fortran program generously provided by J. S. Gallagher at the National Bureau of Standards.

To determine the thermodynamic state after decompression, I assume that decompression takes place adiabatically – that is, that the heat (Q) transferred between the rock/water mixture and its surroundings does not significantly change the total heat of the system. I also assume that expansion and acceleration of the fluid is not significantly dissipated as heat by internal shearing or friction. By implication, then the total change in entropy (dS, $\equiv dQ/T$) is zero. The assumption of isentropic expansion is common in models of eruption dynamics (e.g. Kieffer 1984; Wohletz 1986). (In contrast, modelers of geothermal flow commonly assume that adiabatic expansion takes place isenthalpically (e.g. Stevenson 1993). The assumption of zero enthalpy change in implies that all acceleration is converted to heat by internal shearing and friction (e.g. Liepmann and Roshko 1957, p. 15). It is an appropriate assumption for flow in porous media but not for flow in volcanic conduits). The post-decompression state of the rock/fluid mixture can therefore be defined by its pressure ($=1$ atm) and entropy.

The isentropic assumption makes it especially convenient to use plots of temperature versus entropy to examine paths of decompression (Fig. 3). For liquid water at the boiling point, decompression to atmospheric pressure is represented by a vertical line (e.g. line 1) extending from the left boundary of the bell-shaped curve to the 0.1 MPa isobar. Decompression of water vapor at magmatic or near-magmatic temperature is represented by a vertical line (e.g. line 2) extending from the shaded region on the upper right side of the plot to the 0.1 MPa isobar. Adiabatic decompression of liquid water at the boiling point will always produce a mixture of water and steam. Decompression of water vapor at magmatic temperatures (say, 900–1150° C) from pressures expected at shallow, subsurface depths ($\sim$0.1–10 MPa) will always produce pure water vapor with no condensed water. At higher initial pressures some condensation occurs (Kieffer and Delany 1979), though the minimum initial pressures required for condensation in this temperature range ($P_i = 17$–45 MPa) are higher than one would expect for most shallow-rooted eruptions. At $P_i \leqslant 10$ MPa, $T_i \leqslant 770$° C is required for condensation to occur.

If the erupting mixture consists of both solid particles and fluid, the degree of heat transfer between

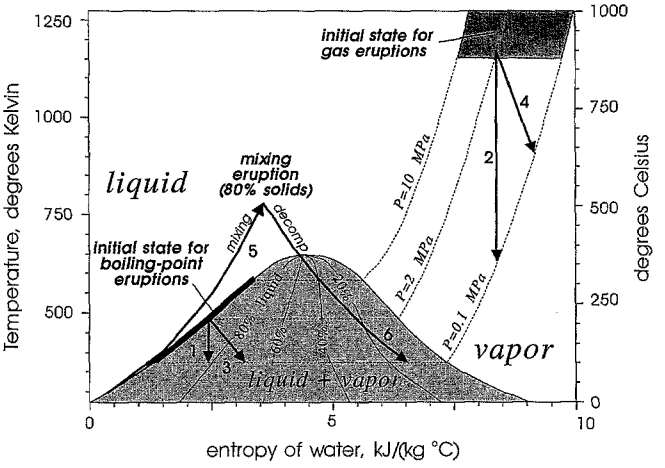

Fig. 3 Plot of temperature versus entropy for liquid water and water vapor showing the initial temperature–entropy states for most fluids involved in gas and boiling-point eruptions and thermodynamic paths of fluids during decompression. The bell-shaped curve in this plot, whose apex is at about 374° C, overlies the region in which liquid water and steam coexist. Steeply dipping lines within this region that converge on the apex are contours of equal mass fraction of steam in a coexisting mixture. Increasing mass fractions of steam extend from left to right on the plot. The area to the right of the bell-shaped region represents pure water vapor. The region to the left represents pure liquid water. Above the bell-shaped curve, water exists as a supercritical fluid whose properties may vary widely. Temperature–entropy paths 1–6 are described in the text

these components during ejection will partly determine the amount of mechanical energy released from a given rock/fluid mixture. The greatest energy release comes from mixtures that are initially at thermal equilibrium and maintain equilibrium during the decompression process. For a mixture of solids and water, lines 3 and 4 represent temperature–entropy paths of the fluid component of the mixtures. They always slope to the right. The slope of such a line is given by the conservation of specific entropy (s) between the solid phase (denoted by subscript r) and fluid phase (subscript w), as the change in specific entropy of the mixture (ds_m) is zero

$$ds_m = 0 = m_r\, ds_r + m_w\, ds_w \tag{5}$$

The change in specific entropy of rock with temperature is (Moran and Shapiro 1992, p. 205)

$$ds_r = \frac{C_r\, dT_r}{T_r} \tag{6}$$

so, substituting Equation (6) into Equation (5), taking the rock temperature (T_r) to be equal to the mixture temperature (T_m), and rearranging, the slope of decompression lines in Fig. 3 is

$$\frac{dT_m}{ds_w} = \frac{-m_w}{m_r}\,\frac{T_m}{C_r} \tag{7}$$

If the solid particles maintain constant thermal equilibrium with the fluids during decompression, then the total change in entropy of the water during decom-

pression can be obtained by rearranging Equation (7) and integrating

$$s_{wf} - s_{wi} = -\frac{m_r}{m_w} C_r \ln \frac{T_{mf}}{T_{mi}} \quad (8)$$

where T_{mi} and T_{mf} denote the initial and final temperatures of the mixture, and s_{wf} and s_{wi} represent final and initial specific entropies of the water, respectively.

Whether in fact the solids and fluids maintain thermal equilibrium during decompression depends largely on the grain size distribution of the rock fragments and on the degree of mixing between the rock fragments and the fluid as they are released. For the solids to maintain approximate thermal equilibrium with the fluid over the time scale of the eruption, fragment diameters must be on the order of a few millimeters or less (Sparks and Wilson 1976). If a significant fraction of erupted material is larger than this (which is the case for most eruptions), heat transfer during the eruption will be incomplete. In addition, many eruptions (e.g. Mastin 1991) derive their solid material from vent walls or from blockages in the vent, which are probably cooler than the initial fluid. The heat contribution of solids in these eruptions would also be less than assumed here.

If the initial temperature and entropy of the solid/fluid mixture are known, and the final temperature of the mixture is known, Equation (8) can be used to solve analytically for the final entropy and hence to determine the thermodynamic state of the final mixture. This task is simple if the final erupted mixture contains coexisting water and steam, the equilibrium temperature of which is 100° C. If the final mixture contains pure steam, however, the final temperature is not known *a priori*. To determine the final thermodynamic state of mixtures under these conditions, the temperature–entropy path was tracked numerically using Equation (7). At each temperature step the equilibrium pressure was calculated using the Fortran program for steam properties described earlier, and the calculation was halted when the $P = 0.1013$ MPa (1 atm) isobar had been reached. Once the final thermodynamic state of the mixture was found, other state variables (internal energy, enthalpy, temperature, specific volume) were determined.

Thermal equilibration in mixing eruptions

To simulate mixing eruptions, the two components were mixed and allowed to thermally equilibrate at constant volume before decompressing. Equilibrium temperatures were obtained by iteratively calculating the following equation from $T_r = T_{rp}$ and $T_w = T_{wp}$ (subscript p denotes pre-mixing temperatures) until $T_r = T_w$ $(= T_{mi})$

$$dT_w = \frac{-m_r C_r}{m_w C_{vw}} dT_r \quad (9)$$

where C_{vw} is the specific heat of water at constant volume. The T–s path of water ($m_r = 0.8$, $T_{rp} = 1150°$ C, $T_{wp} = 25°$ C) during thermal equilibration is shown by line 5 in Fig. 3.

The constant volume assumption implies that no energy is lost to the surroundings (in the form of expansion work) during the mixing process. It should be noted that pressures achieved during constant-volume mixing (frequently GPa) may be orders of magnitude greater than those expected at shallow depth under quasi-static conditions. Under dynamic pressurization, however, very high pressures could be achieved. Some experiments on explosive magma–water mixing (Zimanowski et al. 1991), for example, have measured transient pressures of 50–100 MPa in crucibles with essentially no confinement. Under such conditions, as long as the rate of pressurization is significantly faster than the rate at which pressure can be relieved by shouldering aside the surrounding material, then transient pressures can greatly exceed lithostatic pressure and rock strength.

In phreatomagmatic eruptions, where water mixes with magma rather than with hot rock, and in cases where the magma can crystallize rapidly, then the heat of crystallization of the magma, $m_r h_{xtl}$, would be transferred from the rock to the water before the magma begins to cool. The best documented mixing-type eruptions have involved rock that was initially at a temperature approaching magmatic. The crystallization term is the only term distinguishing such high-temperature eruptions from phreatomaginatic eruptions.

Results

The energy released ($u_i - u_f$) in each of the three types of eruptions is illustrated in Fig. 4. Because of their high initial temperature, gas eruptions are the most energetic of the three types. Under optimal conditions, they can release up to 1.2 MJ/kg of energy – more than half as much as an equivalent mass of gunpowder, and a fourth as much as TNT (Fig. 4b). Mixing eruptions liberate less energy ($\leqslant$360 kJ/kg) and boiling-point eruptions less still ($\leqslant$250–300 kJ/kg).

A second characteristic is that boiling-point and gas eruptions release the most energy when the mass fraction of rock is lowest (Fig. 4). Mixing-type eruptions, in contrast, are most energetic when the mass fraction of rock is fairly high – about 0.8 to 0.9, similar to phreatomagmatic eruptions (Wohletz 1986). For mixing eruptions, the reason for the optimal energy release at high mass fractions of rock is fairly obvious; the rock is the main source of energy in the mixing-type eruptions, whereas it is only one of two energy sources in the other two eruption types (the other source being the fluid). For boiling-point and gas eruptions, the monotonic decrease in energy release with increasing mass fraction of rock is due in part to the fact that the specific heat of water (~3–4.5 kJ/kg °C) is significantly greater than

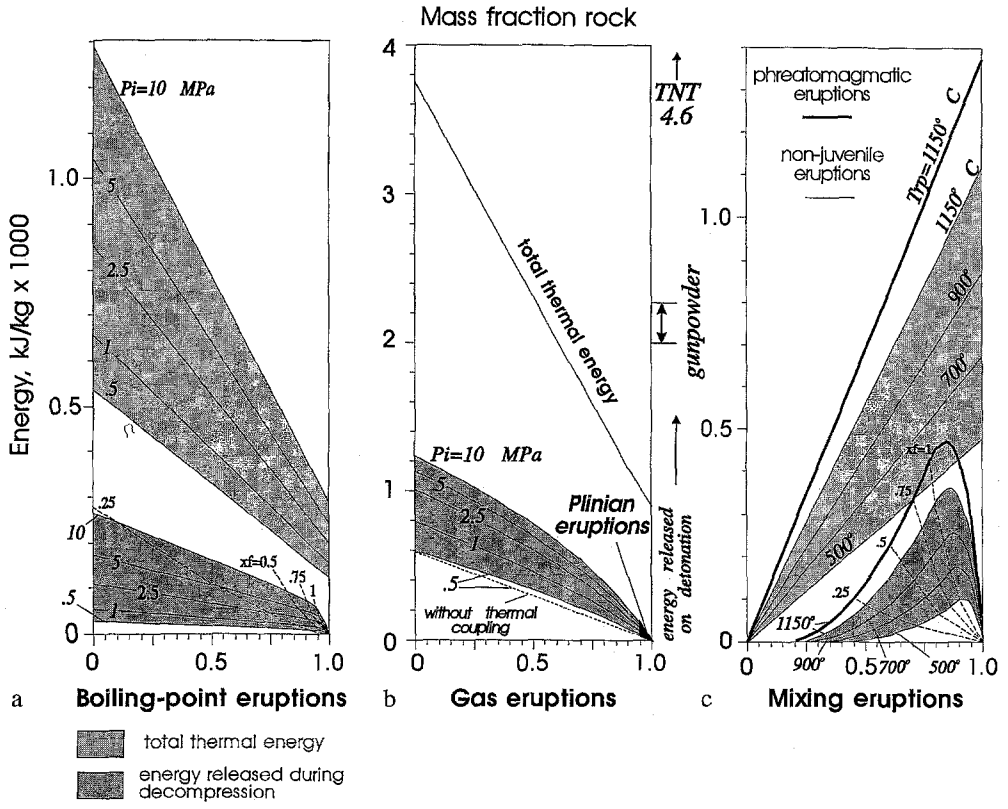

Fig. 4a–c Energy per kilogram of rock/fluid mixture, as a function of mass fraction rock, for **a** boiling-point eruptions, **b** gas eruptions and **c** mixing eruptions. The upper, lightly shaded regions of each plot show initial total thermal energy of rock-fluid mixtures (u_{mi}) in excess of the energy those mixtures would contain at $P=1$ atm, $T=25°C$; the darkly shaded regions show energy released by those mixtures ($u_{mi}-u_{mf}$) during isentropic decompression. By comparison, gunpowder and TNT release ~2–2.3 and 4.6 MJ/kg, respectively, on detonation (plot **b**). All results except for the lowermost, dotted, line in **b** assume complete thermal coupling between fluid and solids during ejection. The dotted line in **b** assumes no cooling of solid material during decompression. In all plots, $C_r=1$ kJ/(kg °C) and $\rho_r=2500$ kg/m^3 and are assumed to be invariant with temperature or pressure. For **b**, $T_{wi}=950°$ C. For **c**, $T_{wp}=25°$ C and, for the phreatomagmatic case, $h_{xtl}=250$ kJ/kg. Broken lines in **a** and **c** indicate final mass fractions steam in the mixtures

that of rock (~1 kJ/kg °C). Thus less energy is given off during adiabatic cooling of rock than water.

As a percentage of the total thermal energy of these mixtures (also shown in Fig. 4), the available energy (u_i-u_f) ranges from 0% (for $m_r=1$) to 20% for boiling-point eruptions (at $m_r=\sim 0.9$), 34% for gas eruptions (at $m_r=\sim 0.3$–0.4) and 38% for mixing eruptions (at $m_r=0.84$). The highest efficiencies occur at high P_i for boiling-point and gas eruptions, and high T_{rp} for mixing eruptions.

Several other relationships are apparent in Fig. 4. For boiling-point eruptions, an increasing percentage of liquid water is converted to steam with increasing mass fraction rock (broken lines, Fig. 4a). The amount of liquid water converted to steam greatly affects the energy release. For m_r less than that required to convert all water to steam, the available energy decreases linearly with m_r. For greater values of m_r, the available energy drops off rapidly because the equilibrium temperature of the final superheated mixture is greater than 100° C and more energy is retained in the final mixture.

For gas eruptions (Fig. 4b), the available energy follows a smoother, monotonic, slightly convex-upward path with increasing mass fraction rock. Plinian eruptions, whose violence is attributed to the expansion of gas bubbles within the melt during decompression, generally contain less than about 5 wt.% volatiles and would plot at the lower end of this scale. In terms of energy released per unit mass of erupted material, they are relatively non-energetic compared with more highly gas-changed mixtures.

One can assess the implications of the assumption that entrained rock is thermally coupled to the expanding fluid by comparing the two bottom lines on Fig. 4b. The lower, broken line decreases exactly linearly with increasing rock fraction and illustrates the energy available when the rock is thermally decoupled from the decompressing mixture. Several workers (Self et al. 1979; Wilson 1980; Wohletz 1986) have taken this scenario as one end-member in estimating the energy release or maximum theoretical velocity of erupting mixtures, referring to it as the 'adiabatic' case (meaning that the fluid alone is decompressing adiabatically). The upper solid line shows the result with complete thermal equilibration between the two components. For our purposes, the difference is insignificant. Results for partial thermal equilibration would plot between the two lines.

In boiling-point eruptions, the importance of thermal coupling is much greater, due to the fact that the energy versus m_r curves are more non-linear between $m_r=0$ and $m_r=1$. The greatest difference in energy release between thermally coupled and uncoupled mixtures occurs at $m_r=0.90$–0.98. For these values of m_r, thermally uncoupled mixtures release only 8 to 34% as much energy as thermally coupled mixtures, with the lowest percentages occurring in the mixtures with the lowest initial pressures.

A second end-member has been taken by various workers examining pressure–velocity relationships of erupting mixtures (Self et al. 1979; Wilson 1980) – that is, that gas decompresses isothermally. This assumption is entirely appropriate for velocity studies of mixtures containing high mass fractions of small solid particles, because $T_i = \sim T_f$ for those mixtures. It produces a zero or negative energy release (i.e. $u_f \geqslant u_i$), however, and therefore is not an appropriate approximation when calculating energetics.

Mixing eruptions (Fig. 4c) that involve rock at nearly magmatic temperatures produce eruption energies that are less than those of phreatomagmatic eruptions by only about 10–20%. As mentioned earlier, this difference is due entirely to the crystallization energy of magma (h_{xtl}). According to my analysis, the optimal energy produced by mixing magma at 1150° C ($h_{xtl}=250$ kJ/kg, $C_r=1$ kJ/kg° C) with water at 25° C occurs at $m_r = \sim 0.84$, or $m_r/m_w = \sim 5.2$. This value is similar to values obtained by Wohletz (1986) ($m_r/m_w = \sim 5.5$ from theory; $m_r/m_w = \sim 3$ from experiments). For rock, optimal mass fractions are slightly greater: $m_r=0.87$, 0.88 and 0.92 for initial rock temperatures of 900, 700 and 500° C, respectively. These peaks in available energy occur at a mass fraction of rock about 0.10 greater than the minimum required to convert all available water to steam. The positions of the energy maxima are a result of two competing factors: the increasing amount of energy contributed by rock at higher values of m_r, and the increasing amount of heat retained in the final, decompressed mixture with increasing m_r, once the final mass fraction steam (x_f) reaches unity.

Results in terms of energy liberated per unit *volume* of pre-erupted fluid/rock mixture (Fig. 5) are quite different from those expressed in energy per kilogram. For mixing eruptions, mechanical energy release ranges up to more than 700 MJ/m^3, for boiling-point eruptions to only about 200 MJ/m^3 and for gas eruptions less than 40 MJ/m^3 (a maximum that, interestingly, occurs when $m_r = \sim 0.8$).

What can one infer about the characteristics of different types of eruptions from these results? I speculate that the energy release per unit mass may be relevant to the question of eruptive violence, whereas the energy release per unit volume may partially constrain the maximum eruptive size. Gas eruptions can eject a given mass of material more energetically than any other eruption type, but the gas reservoir that powers the eruptions will be depleted rapidly. One might therefore

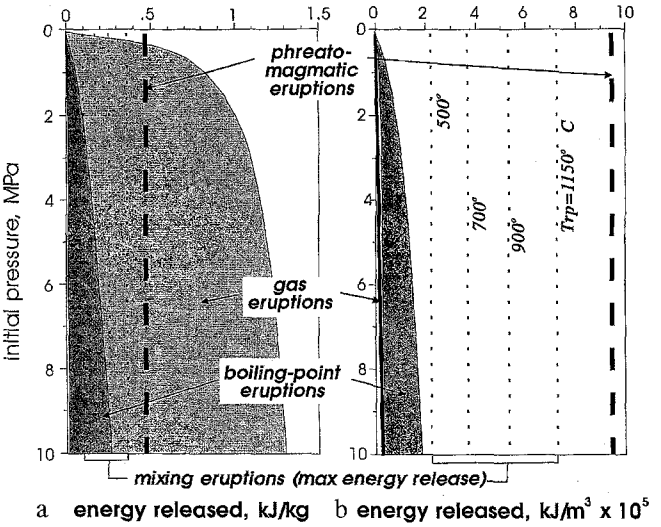

Fig. 5 **a** Mechanical energy release per kilogram of rock/fluid mixture for the three types of eruptions. Heavily stippled field shows energy release from boiling-point eruptions with $m_r=0$ (right-hand side) to 0.99 (left-hand side). Lightly stippled field shows the same relationship for gas eruptions. Short-dashed vertical lines represent the maximum energy released in mixing eruptions with water ($T_{wp}=25$° C) and rock ($C_r=1$ kJ/kg° C, $\rho_r=2500$ kg/m^3) at initial temperatures of, from left to right, 500, 700, 900 and 1150° C. The long-dashed vertical line on the right represents the maximum energy released from phreatomagmatic eruptions, with $T_{rp}=1150$° C, $T_{wp}=25$° C and $h_{xtl}=250$ kJ/kg. **b** Same as plot **a**, except that energy release is expressed per unit volume pre-erupted mixture rather than per unit mass

expect gas eruptions to be small and violent, whereas boiling-point and mixing eruptions would be (under optimal conditions) less violent but potentially larger. The few reasonably well-documented examples of gas eruptions (e.g. Galeras 1993) appear to follow this model. They produce explosive eruptions with relatively high eruptive velocities, short duration and small total erupted volumes.

Final temperatures and mass fractions steam

Figure 6 illustrates the variations in final temperature (T_f) and mass fraction of steam (x_f) for erupted mixtures from the three types of eruptions. As mentioned earlier, gas eruptions whose initial temperatures are greater than 770° C and pressures less than 10 MPa do not condense when decompressing to atmospheric pressure. At initial temperatures as low as 400° C (26° C above the critical point of water), gas eruptions with $P_i=10$ MPa (Fig. 6a) could condense up to 20% of their water. Boiling-point eruptions, on the other hand, do not convert more than about 50% of their water to steam until the mass fractions of rock exceed about 0.7. If water and rock are thermally decoupled during decompression, the values of x_f at $m_r=0$ in Fig. 6a represent x_f for all m_r. For $P_i \leqslant 10$ MPa, they do not exceed $x_f=0.35$ (left-hand side of Fig. 6a). This agrees with ob-

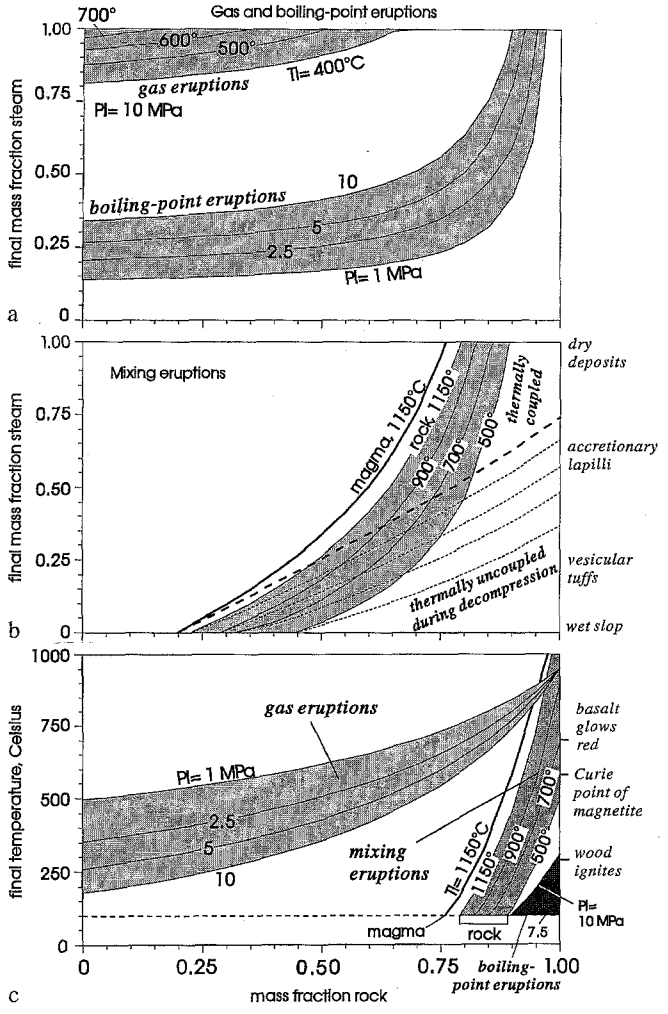

Fig. 6a–c Final mass fraction steam (x_f) in erupted mixtures for **a** gas and boiling-point eruptions, **b** mixing eruptions and **c** final temperature of erupted mixtures (T_f) for all three types of eruptions. $T_{wi}=950°$ C for gas eruptions. To the right of **b** are deposit textures that indicate relative water content (Fisher and Schmincke 1984; Rosi 1992). To the right of **c** are various temperature indicators (sources are Hoadley 1980, for wood ignition; Telford et al. 1976, for the magnetite Curie point; Decker and Christiansen 1984, for the incandescence of basalt)

servations from most hydrothermal eruptions, which typically involve very muddy deposits (e.g. White 1955), sometimes with soft sediment deformation or even mobilization of the deposits as debris flows (Marini et al. 1993), although, as mentioned earlier, some hydrothermal eruptions include relatively dry stages. Deposits from boiling-point eruptions that are dry throughout the duration of the eruption should be (and appear to be, based on published accounts) rare.

For mixing eruptions (Fig. 6b), x_f is much more highly variable than for gas or boiling-point eruptions. If water and rock are thermally coupled during decompression, $x_f=1$ for m_r greater than about 0.75–0.9. If rock and water are thermally decoupled, not more than about 70% of the water is converted to steam for $m_r \leqslant 0.99$. For mass fractions of rock less than about 0.2–0.45 (depending on the initial temperature of the rock), the water never boils and eruptions are impossible. Deposits of phreatomagmatic eruptions exhibit textures indicating a complete range of water contents (Fisher and Schmincke 1984). Deposits of mixing eruptions are less well documented, but the few published descriptions (e.g. Moyer and Swanson 1987; McPhie et al. 1990) appear to show a similarly wide range of water contents.

Final temperatures of erupted mixtures vary considerably depending on m_r and eruption type. As shown in Fig. 6c, the final temperature of boiling-point mixtures does not exceed 100° C until $m_r \geqslant \sim 0.9$. A final temperature great enough to ignite wood ($\sim 280°$ C, Hoadley 1980), as observed at Rotomahana in 1886 (Nairn 1979) would require an unusually high initial pressure, high m_r and complete thermal coupling, and is unlikely to occur.

At high values of m_r, both gas and mixing eruptions are capable of expelling mixtures at nearly magmatic temperatures. The expulsion of incandescent rock fragments or glowing dust clouds in non-juvenile eruptions (e.g. Decker and Christiansen 1984; Smithsonian Institution 1992) is a certain indicator that the initial temperatures were well above the boiling point.

Maximum theoretical velocities

These results have implications regarding the form in which the energy from these eruptions may be released. In very simplistic terms, the forms of energy released per mass of erupted debris can be accounted for as

$$-\mathrm{d}u_m = \mathrm{d}(Pv_m) + g\mathrm{d}z + \mathrm{d}\left(\frac{v^2}{2}\right) + \text{'external frictional terms'} \quad (10)$$

where $\mathrm{d}(Pv_m)$ is the change in energy associated with expansion and decompression of the mixture (v_m is the specific volume of the mixture); $g\mathrm{d}z$ is the work required to lift the mixture and $\mathrm{d}(v^2/2)$ is the change in specific kinetic energy of the mixture (v is velocity). The external frictional terms include all other forms of energy transferred from the erupting mixture to the surroundings, including seismic waves in the earth, inelastic deformation or breakage of country rock, and shock waves. This equation is a modification of Bernoulli's equation (not to be confused with the modified Bernoulli equation used by Fudali and Melson (1972) and others to relate pressure and velocity), with the addition of frictional terms and the specific internal energy. Because enthalpy, h, is by definition $(u+Pv)$, the terms can be rearranged and integrated to give the following equation

$$h_{mi} - h_{mf} = g(z_f - z_i) + \tfrac{1}{2}(v_f^2 - v_i^2) + \text{'external frictional terms'} \quad (11)$$

The lifting work, $g(z_f - z_i)$ (~ 1 kJ/kg for 100 m of lifting), is normally a small part of the total energy re-

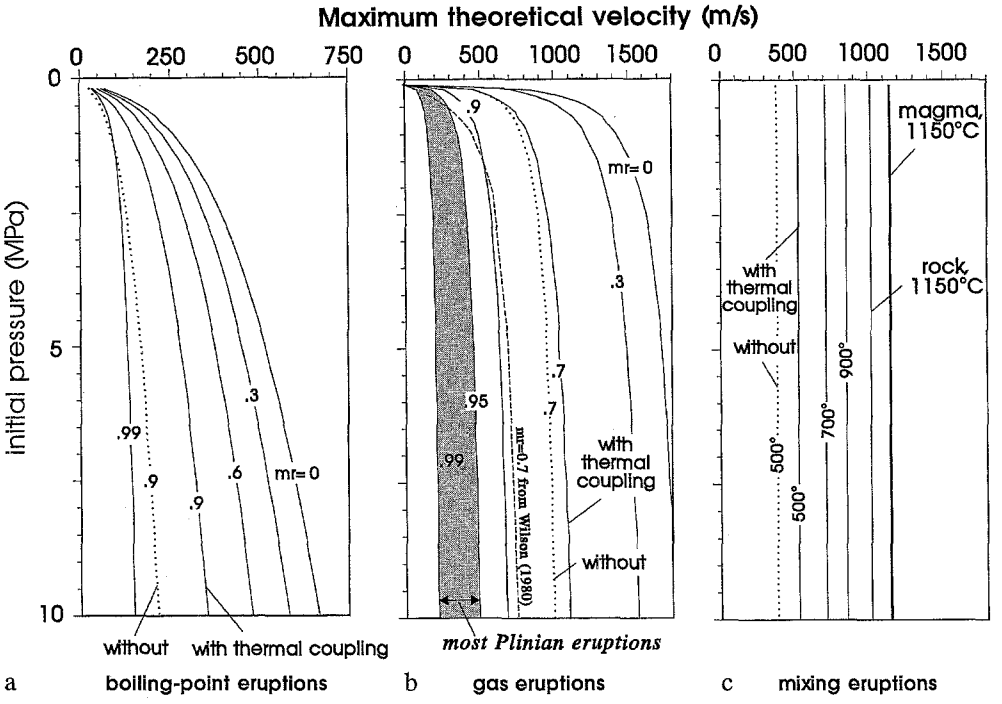

Fig. 7a–c Maximum theoretical velocity versus initial pressure for **a** boiling-point eruptions, **b** gas eruptions ($T_i = 950°$ C) and **c** mixing eruptions ($T_{wp} = 25°$ C, for optimal values of m_r). For mixing eruptions, maximum theoretical velocities are plotted as a function of pressure of rock and water before mixing. Theoretical velocities are nearly independent of this parameter. Broken line in middle plot indicates maximum theoretical velocities calculated by Wilson (1980) for vulcanian eruptions with $m_r = 0.70$

leased (hundreds to thousands of kJ/kg). Thus by assuming $v_i = 0$ and neglecting the lifting and friction terms, a maximum theoretical velocity (v_{max}) can be obtained

$$v_{max} = \sqrt{2(h_{mi} - h_{mf})} \tag{12}$$

This assumes that all mechanical energy in the eruption goes into the expansion and acceleration of the mixture. It also assumes that the rock mixture accelerates uniformly and is not significantly slowed by drag against the walls of the vent or the atmosphere.

Because v_{max} depends on the state variable h, which in turn depends on the initial pressure, this equation can be thought of as relating the maximum potential velocity to the initial pressure of a rock/fluid mixture. Figure 7 shows the relationship between initial pressure and maximum theoretical velocity for the three types of eruptions. Maximum theoretical velocities for gas eruptions range up to a remarkable 1800 m/s and are at least a few times higher than for boiling-point eruptions at comparable values of m_r and P_i. Under optimal conditions, theoretical velocities for mixing eruptions are somewhere in between those of gas and boiling-point eruptions. For both boiling-point and gas eruptions, maximum theoretical velocities are significantly higher for low values of m_r than for high values. In fact, v_{max} for $m_r \leqslant \sim 0.95$ are higher than has ever been observed. This point will be discussed in more detail below.

If the solid fraction transfers no heat to the fluid during expansion, the enthalpy change of the fluid would be identical to that when $m_r = 0$, but this enthalpy change would be used to accelerate the entire mixture. Thus the maximum theoretical velocity at $m_r = n$ would be

$$(v_{max})_{mr=n} = \sqrt{2 m_w (h_{mi} - h_{mf})_{mr=0}} \tag{13}$$

For gas eruptions, the difference between theoretical velocities with thermal coupling (solid lines, Fig. 7b) and without thermal coupling (dotted line) is rather small ($< \sim 12\%$), and is greatest when $m_r = \sim 0.7$. For boiling-point eruptions, the difference is greatest (up to about 45%) when $m_r = 0.9$–0.95. For mixing eruptions, the difference is greatest at lower values of T_{rp}, with uncoupled maximum velocities about 27% below coupled velocities at $T_{rp} = 500°$ C.

For eruptions or explosions involving gas and magma or rock at magmatic temperatures, previous workers (e.g. Self et al. 1979; Wilson 1980; Fagents and Wilson 1993) have attempted to relate eruptive velocities to pressures within eruptive vents or lava domes. Wilson (1980) estimated maximum theoretical velocities in plinian eruptions by assuming an isentropically expanding mixture of solid particles in an ideal gas. His maximum theoretical velocities are very similar to those of this study. Wilson (1980) and Self et al. (1979) also estimated maximum theoretical velocities for vulcanian eruptions, which they idealized as rapid ejection of a cap of solidified magma above a chamber of adiabatically expanding ideal gas within a volcanic conduit. In contrast with my analysis, theirs takes into account air drag on the rock cap and assumes no heat transfer from solid to fluid during expansion. Their calculated velocities (e.g. broken line, Fig. 7b) are lower than those presented here. Their analysis may be more appropriate than mine for the initial stage of vulcanian eruptions, though they acknowledge that even in the initial stages, air drag on blocks is less than would be calculated using their assumption of still air above the vent. Fagents and Wilson (1993) have modified the original model of Wil-

Table 1 Eruption velocities estimated from selected gas and steam-blast eruptions

Country	Volcano	Start date	End date	Maximum velocity (m/s)	Estimation method	Inferred cause	Reference
W. Indies	Soufriere de Guadeloupe	Jul 1976	Mar 1977	30–150	Photos	Boiling-point	Le Guern et al. (1980)
New Zealand	Kawerau	14.5 ka	9 ka	150–200	Horiz. dist.	Boiling-point	Nairn and Wiradiradja (1980)
New Zealand	Tauhara	20 Jun 1981	20 Jun 1981	90–100	Horiz. dist.	Boiling-point	Scott and Cody (1982)
New Zealand	Waiotapu	<1.8	<1.8	50–150*	Horiz. dist.	Boiling-point	Hedenquist and Henley (1985)
USA	Inyo Craters	0.55 ka	0.55 ka	80–100	Horiz. dist.	Boiling-point?	Mastin (1991)
Costa Rica	Arenal+	29 Jun 1968	29 Jun 1968	~325–400+	Horiz. dist.	Gas	Fudali and Melson (1972), Fagents and Wilson (1993)
Japan	Sakurajima+	May 1982	Nov 1982	112/157	Photos	Gas	Ishihara (1985)
Japan	Asama+	Apr 1935	Jun 1938	130–210	Horiz. dist.	Gas	Minakami (1942)
New Zealand	Ngauruhoe+	Feb 1975	Feb 1975	~400	Photos	Gas	Nairn and Self (1978)
USA	Mt St Helens	Dec 1989	Feb 1991	40–80	Horiz. dist.	Gas	Mastin (1994)
USA	Kilauea	May 1924	Jun 1924	~ 75	Horiz. dist.	Mixing	L. G. Mastin (unpublished data)
USA	Kilauea	1790	1790	~175	Horiz. dist.	Mixing?	L. G. Mastin (unpublished data)
USA	Mt St Helens	May 1980	Dec 1982	15–25	Photos	Mixing	Moyer and Swanson (1987)

* This is Hedenquist and Henley's estimate of velocity of large blocks. Finer debris may have had velocities of 150–350 m/s

+These were technically not non-juvenile eruptions, but were driven primarily by magmatic gas

+Original estimates of 600 m/s by Fudali and Melson (1972) and Wilson (1972) were revised downward by Fagents and Wilson (1993)

son (1980) to account for reduced air drag. Once the eruption has become established, air drag is not important and the calculated velocities in this paper are a more realistic maximum.

Table 1 lists the ejection velocities calculated or estimated from large blocks for several gas and steam-blast eruptions, and for the initial stages of a few vulcanian eruptions. For boiling-point and mixing eruptions, velocities estimated from photographs or ballistic studies range from tens of meters per second to more than 200 m/s. Significantly higher velocities (up to ~400 m/s) have been inferred for mixtures of fluid and fine solid particles (e.g. Nairn and Wiradiradja, 1980). These estimates are based on the assumption that the large blocks were falling at terminal velocity through the rock/fluid mixture at the time of ejection, and that the density of the mixture was on the order of 1 kg/m^3. Densities of these mixtures are very poorly constrained. They could have been nearly as high as the blocks themselves if blocks and debris were ejected en masse at the beginning of the eruption, in which case the block velocities would have equaled the rock/fluid mixture velocities. For gas and vulcanian eruptions, maximum velocities range up to about 400 m/s. Observed velocities agree with maximum theoretical velocities (Fig. 7) only if we assume that m_r for those eruptions was greater than about 0.9, or that initial pressures were less than ~0.2 MPa (for gas eruptions) or ~0.5 MPa for boiling-point eruptions. High m_r probably accounts for most of the relatively low observed velocities: as described by numerous observers (e.g. Fudali and Melson 1972; Nairn and Self 1978; Self et al. 1979), velocity estimates are generally made from ballistic fragments ejected at the inception of an eruption, when the concentration of solid debris is high. Later stages in gas and steam-blast eruptions frequently emit jets of nearly ash-free fluid (e.g. White 1955; Smithsonian Institution 1992, 1993). Owing to lower concentrations of solid debris in the mixture, eruption velocities during these latter stages should be much higher than initial velocities, though few (if any) observations have been made to verify this.

A number of other factors could be responsible for the fact that observed velocities are much less than the theoretical maxima. Two important ones are choked flow and frictional flow, described in the following.

Effect of choked flow on eruptive velocities. If the initial pressure of the erupting mixture is more than about twice atmospheric pressure, the erupting mixture will reach its sonic velocity at the narrowest point in the conduit and the mixture velocity above that point will be controlled largely by the conduit geometry (e.g. Saad 1985, p. 87; Kieffer 1984). For a mixture of steam and rock (T_{mi}=950° C), sonic velocities range from ~100 m/s for m_r=0.99 to 800 m/s for m_r=0. For rock/steam/water mixtures at boiling-point temperatures, sonic velocities can range from a few meters per second (for low x, Kieffer 1977, and high m_r) to about 500 m/s (for x= ~1 and m_r= ~0, Haar et al. 1984). If the conduit is most constricted at the surface, these will be the exit velocities. If the vent opens above the constriction but doesn't not flare sufficiently to allow the mixture to expand to atmospheric pressure, it will be *overpressured* once it exits (Kieffer 1984). Excess enthalpy will be dissipated by the production of oblique shock waves and lateral expansion of the gas, increasing entropy and decreasing velocities below those predicted by Equa-

tion (12). Alternatively, if the vent flares more than is required for the gas to decompress to atmospheric pressure, a stationary shock wave will develop within the vent, downstream of which entropy will increase and velocities will abruptly drop to subsonic values. Exit velocities from most eruptive vents probably range from sonic velocities to the isentropic maximum values calculated in this paper.

Effect of friction and turbulence on eruptive velocities. Although friction has thus far been neglected, all flow in conduits is reduced to some extent by friction between the fluid and the conduit walls, and by internal shearing and turbulence. Fluids that flow through porous media or through long, circuitous pathways (e.g. in hydrothermal systems) can dissipate essentially all of their kinetic energy through internal friction, resulting in isenthalpic, or 'throttled' flow (Liepmann and Roshko 1957, p. 15). Fluids that flow through short, smooth ducts (e.g. steam nozzles; Moran and Shapiro 1992, p. 234), commonly accelerate to within a few per cent of theoretical isentropic velocities. Numerous experiments have produced a wealth of data on frictional resistance to flow in conduits (e.g. Saad 1985, p. 192). For ideal gases (or 'pseudogases', Kieffer 1984) flowing through conduits of constant cross-sectional area, exit flow properties can be calculated from closed-form solutions using friction factors taken from experimental data (Saad 1985, pp. 200–205). These solutions indicate that an erupting mixture modeled as a pseudogas (Kieffer 1984) with $T_i = 950°$ C, $P_i = 1$–10 MPa, $m_r = 0$–0.99, in a conduit with friction factors appropriate for volcanic conditions (~ 0.01, Buresti and Casarosa 1989) and conduit length/diameter ratios (H/D) of ~ 1–10, would erupt with velocities within several per cent of v_{max}. For H/D of ~ 100, velocities are still within a few tens of per cent of v_{max}. One might expect qualitatively similar results for real erupting mixtures.

Discussion and conclusions

All assumptions in this study, in particular those relating to isentropic decompression, thermal coupling of rock and fluid and constant-volume conditions of rock and water during thermal equilibration, maximize the amount of energy converted to work during the eruption. If these conditions are not met, the results could change in one of two ways: (1) less energy may be converted to work or (2) the energy may be converted to work, but not in the forms (acceleration, expansion, and lifting) prescribed under the non-frictional terms in Equation (11). Incomplete heat transfer from rock to fluid, for example, either during mixing (in mixing eruptions) or during decompression, means that, at the end of decompression, the erupting mixture will have a greater heat content and will have converted less energy to work. If heat is concentrated in the smaller particles, it may still be converted to work by driving convection in the eruptive plume. If it is contained in the larger clasts that fall out of the plume, on the other hand, it may be transferred to the ground and the atmosphere without any significant work being done. Similarly, if friction and turbulence reduce the velocities in the vent during the eruption, they will tend to reduce the kinetic energy of the final mixture, but increase the heat content of the decompressed fluid, resulting either in increased convective uplift or increased distribution of heat around the vent during fallout of clasts.

The effects of friction, incomplete heat transfer, block fallout, choked flow and turbulence, among other factors, can be dealt with more quantitatively if one makes assumptions (or has direct observational information) regarding pyroclast size distributions, conduit geometry and, for mixing eruptions, conditions under which mixing took place. Numerical models that include these processes will be the subject of future studies.

Acknowledgements This paper was improved greatly by careful reviews from Ken Wohletz and Steve Ingebritsen, and by helpful comments from Sue Kieffer, Lionel Wilson and Steve Self.

References

Bacon CR (1983) Eruptive history of Mount Mazama and Crater Lake caldera, Cascade Range, U.S.A. J Volcanol Geotherm Res 18:57–115

Bercich BJ, McKibbin R (1992) Modelling the development of natural hydrothermal eruptions. Proc 14th NZ Geoth Workshop 1992, pp 305–312, and corrigendum, Proc 15th NZ Geoth Workshop 1993, University of Auckland, Auckland, New Zealand, pp 345–346

Bixley PF, Browne PRL (1988) Hydrothermal eruption potential in geothermal development. Proc 10th New Zealand Geothermal Workshop, University of Auckland, Auckland, New Zealand, pp 195–198

Browne PRL, Lloyd EF (1986) Water dominated geothermal systems and associated mineralisation. In: Taupo Volcanic Zone: Tour Guides C1, C4, C5, and A2, New Zealand Geol Survey Record 11:145–212

Buresti G, Casarosa C (1989) One-dimensional adiabatic flow of equilibrium gas-particle mixtures in long vertical ducts with friction. J Fluid Mech 203:251–272

Burnham CW (1979) Magmas and Hydrothermal Fluids. In: Barnes HL (ed) Geochemistry of Hydrothermal Ore Deposits. Wiley, New York, pp 71–136

Decker RW, Christiansen RL (1984) Explosive eruptions of Kilauea Volcano, Hawaii. In: Explosive Volcanism: Inception, Evolution, and Hazards. National Academy Press, Washington, pp 122–132

Dowden J, Kapadia P, Brown G, Rymer H (1991) Dynamics of a geyser eruption. J Geophys Res 96:18059–18071

Fagents SA, Wilson L (1993) Explosive volcanic eruptions; VII, The ranges of pyroclasts ejected in transient volcanic explosions. Geophys J Int 113:359–370

Finch RH (1943) Lava surgings in Halemaumau and the explosive eruptions in 1924. The Volcano Letter 479:1–4

Fink JH, Anderson SW, Manley CR (1992) Textural constraints on effusive silicic volcanism: beyond the permeable foam model. J Geophys Res 97:9073–9083

Fisher RV, Schmincke H-U (1984) Pyroclastic Rocks. Springer-Verlag, Berlin, pp 1–472

Francis P, Self S (1983) The eruption of Krakatau. Sci Am 249:172–187

Fudali RF, Melson WG (1972) Ejecta velocities, magma chamber pressure and kinetic energy associated with the 1968 eruption of Arenal Volcano. Bull Volcanol 35:383–401
Goguel J (1956) Le mécanisme des explosions phréatiques: Pub Bur Central Seismol Int Ser A, Trav Sci 19:165–175
Haar L, Gallagher JS, Kell GS (1984) NBS/NRC Steam Tables. Hemisphere, New York, pp 1–320
Hedenquist JW, Henley RW (1985) Hydrothermal eruptions in the Waiotapu geothermal system. Econ Geol 80:1640–1688
Hildreth W (1983) The compositionally zoned eruption of 1912 in the Valley of Ten Thousand Smokes, Katmai National Park, Alaska. J Volcanol Geotherm Res 18:1–56
Hoadley RB (1980) Understanding Wood. Taunton Press, Newtown, pp 1–256
Ingebritsen SE, Rojstaczer SA (1993) Controls on geyser periodicity. Science 262:889–891
Ishihara K (1985) Dynamical analysis of volcanic explosion. J Geodyn 3:327–349
Jaggar TA (1949) Steam blast volcanic eruptions. Hawaii Volc Obs, 4th Spec Rep
Kiefer G (1981) Les explosions phréatiques et phréatomagmatiques terminales a l'Etna. Bull Volcanol 44:655–660
Kieffer SW (1977) Sound speed in liquid–gas mixtures: water–air and water–steam. J Geophys Res 82:2895–2904
Kieffer SW (1984) Factors governing the structure of volcanic jets. In: Explosive Volcanism, Inception, Evolution, and Hazards. National Academy Press, Washington DC, pp 143–157
Kieffer SW, Delany JM (1979) Isentropic decompression of fluids from crustal and mantle pressures. J Geophys Res 84:1611–1620
Le Guern F, Bernard A, Chevrier RM (1980) Soufriere of Guadeloupe 1976–1977 eruption-mass and energy transfer and volcanic health hazards. Bull Volcanol 43:578–592
Liepmann HW, Roshko A (1957) Elements of Gasdynamics. Wiley, New York, pp 1–439
Lloyd EF, Keam RF (1974) Trinity Terrace hydrothermal eruption, Waimangu, New Zealand. N Z J Sci 17:511–528
Long PE (1989) Interaction of basalt flows with water during emplacement and solidification [abstract]. In: Proc 1989 IAVCEI Mtg, Santa Fe, NM, p 166
MacDonald GA (1972) Volcanoes. Prentice-Hall, Englewood Cliffs, pp 1–510
Marinelli G (1969) Some geological data on the geothermal areas of Tuscany. Bull Volcanol 33:319–333
Marini L, Principe C, Chiodini G, Cioni R, Fytikas M, Marinelli G (1993) Hydrothermal eruptions of Nisyros (Dodecanese, Greece). Past events and present hazard. J Volcanol Geotherm Res 56:71–94
Mastin LG (1991) The roles of magma and groundwater in the phreatic eruptions at Inyo Craters, Long Valley Caldera, California. Bull Volcanol 53:579–596
Mastin LG (1994) Explosive tephra emissions at Mount St. Helens, 1989–1991: the violent escape of magmatic gas following storms? Geol Soc Am Bull 106:175–185
McPhie J, Walker GP, Christiansen RL (1990) Phreatomagmatic and phreatic fall and surge deposits from explosions at Kilauea volcano, Hawaii, 1790 A.D.: Keanakakoi Ash Member. Bull Volcanol 52:334–354
Minakami T (1942) On the distribution of volcanic ejecta (Part I). The distributions of volcanic bombs ejected by the recent explosions of Asama. Bull Earthquake Res Inst, Tokyo 20:65–91
Moran MJ, Shapiro HN (1992) Fundamentals of Engineering Thermodynamics, 2nd edn. Wiley, New York, pp 1–804
Moyer TC, Swanson DA (1987) Secondary hydroeruptions in pyroclastic-flow deposits: examples from Mount St. Helens. J Volcanol Geotherm Res 32:299–319
Muffler LJP, White DE, Truesdell AH (1971) Hydrothermal explosion craters in Yellowstone National Park. Geol Soc Am Bull 82:723–740
Nairn IA (1979) Rotomahana–Waimangu eruption, 1886: base surge and basalt magma. N Z J Geol Geophys 22:363–378
Nairn IA, Self S (1978) Explosive eruptions and pyroclastic avalanches from Ngauruhoe in February 1975. J Volcanol Geotherm Res 3:39–60
Nairn IA, Wiradiradja S (1980) Late Quaternary hydrothermal explosion breccias at Kawerau Geothermal Field, New Zealand. Bull Volcanol 43:1–13
Nairn IA, Wood CP, Hewson CAY (1979) Phreatic eruptions of Ruapehu: April 1975. N Z J Geol Geophys 22:155–173
Nelson CE, Giles DL (1985) Hydrothermal eruption mechanisms and hot spring gold deposits. Econ Geol 80:1633–1639
Perret FA (1937) The eruption of Mt. Pelee, 1929–1932. In: Carnegie Inst Wash Publ 458, p 126
Rosi M (1992) A model for the formation of vesiculated tuff by the coalescence of accretionary lapilli. Bull Volcanol 54:429–434
Saad MA (1985) Compressible Fluid Flow. Prentice-Hall, Englewood Cliffs, pp 1–560
Self S, Wilson L, Nairn IA (1979) Vulcanian eruption mechanisms. Nature 277:440–443
Smithsonian Institution (1992) Galeras (Colombia) explosion kills 9 people on the active cone, including 6 volcanologists. Bull Global Volcanism Network 17(12):2–4
Smithsonian Institution (1993) Santiaguito (Guatemala) lava effusion and frequent explosions. Bull Global Volcanism Network 18(11):3–6
Sparks RSJ, Wilson L (1976) A model for the formation of ignimbrite by gravitational column collapse. J Geol Soc London 132:441–451
Stearns HA, MacDonald GA (1946) Geology and ground-water resources of the island of Hawaii. Hawaii Div Hydrogr Bull 9:1–363
Stevenson DS (1993) Physical models of fumarolic flow. J Volcanol Geotherm Res 57:139–156
Stix J, Zapata JA, Calvache M, Cortés GP, Fischer TP, Gómez D, Narvaez L, Ordoñez M, Ortega A, Torres R, Williams SN (1993) A model of degassing at Galeras Volcano, Colombia, 1988–1993. Geology 21:963–967
Telford WM, Geldart LP, Sheriff RE, Keys DA (1976) Applied Geophysics. Cambridge University Press, Cambridge, pp 1–860
White DE (1955) Violent mud-volcano eruptions of Lake City Hot Springs, northeastern California. Geol Soc Am Bull 66:1109–1130
White DE (1967) Some principles of geyser activity, mainly from Steamboat Springs, Nevada. Am J Sci 265:641–684
Wilson L (1972) Explosive volcanic eruptions – II. The atmospheric trajectories of pyroclasts. Geophys J R Astron Soc 30:381–392
Wilson L (1980) Relationships between pressure, volatile content and ejecta velocity in three types of volcanic explosion. J Volcanol Geotherm Res 8:297–313
Wohletz KH (1986) Explosive magma–water interactions: thermodynamics, explosion mechanisms, and field studies. Bull Volcanol 48:245–264
Wolfe EW, Hoblitt RP. Overview of the eruptions. In: Newhall CG, Punongbayan RS (eds) Eruptions and Lahars at Mount Pinatubo, Philipines. US Geol Surv Prof Pap, in press
Zimanowski B, Fröhlich G, Lorenz V (1991) Quantitative experiments on phreatomagmatic explosions. J Volcanol Geotherm Res 48:341–348
Zlotnicki J, Boudon G, Le Mouel J-L (1992) The volcanic activity of La Soufriere of Guadeloupe (Lesser Antilles): structural and tectonic implications. J Volcanol Geotherm Res 49:91–104

Editorial responsibility: J. McPhie